

The MC-QTAIM analysis reveals an exotic bond in the coherently quantum superposed Malonaldehyde

Mohammad Goli¹ and Shant Shahbazian^{2,*}

¹School of Nano Science, Institute for Research in Fundamental Sciences (IPM), Tehran
19395-5531, Iran,

Email: m_goli@ipm.ir

²Department of Physics, Shahid Beheshti University, Evin, Tehran, Iran,

E-mail: sh_shahbazian@sbu.ac.ir

Abstract

The proton between the two oxygen atoms of the malonaldehyde molecule experiences an effective double-well potential in which the proton's wavefunction is delocalized between the two wells. Herein we employed the state-of-the-art multi-component quantum theory of atoms in molecules partitioning scheme to obtain the molecular structure, i.e. atoms in molecules and bonding network, from the superposed ab initio wavefunctions of malonaldehyde. In contrast to the familiar clamped-proton portrayal of malonaldehyde, in which the proton forms a hydrogen basin, for the superposed states the hydrogen basin disappears and two novel hybrid oxygen-hydrogen basins appear instead, with an even distribution of the proton population between the two basins. The interaction between the hybrid basins is stabilizing thanks to an unprecedented mechanism. This involves the stabilizing classical Coulomb interaction of the one-proton density in one of the basins with the one-electron density in the other basin. This stabilizing mechanism yields a bond foreign to the known bonding modes in chemistry.

Keywords: Malonaldehyde; Atoms in Molecules; Quantum superposition, exotic bonds

I. Introduction

The superposition principle is probably the most important principle of quantum mechanics with many theoretical ramifications like the exotic quantum correlations and the entanglement, which are quite intriguing from the classical physicist viewpoint.^{1,2} In quantum chemistry and the electronic structure theory the superposition principle manifests itself by various linear combinations of atomic orbitals,³ molecular orbitals,⁴ and Slater determinants.^{5,6} However, the majority of these manifestations include only the electronic states which are derived from the electronic Hamiltonian that treats electrons as quantum particles and the nuclei as clamped point charges. Although it is generally highlighted that the electronic Hamiltonian is just an approximation based on the adiabatic separation of the electronic and nuclear motions,⁷ its almost-universal computational usage conceals its basic shortcoming, namely the total dismissal of the superposition of the nuclear states.^{8,9}

To consider the superposed nuclear states, one may solve the nuclear Schrödinger equation using the potential energy surface (PES) derived from the solution of the electronic Schrödinger equation.¹⁰ However, this approach has rarely been used to challenge the viewpoint of the concept of “molecular structure” in which electrons are delocalized throughout the molecule while nuclei are conceived as point charges vibrating locally around their equilibrium positions.¹¹⁻¹⁴ Some simple examples that may challenge this prototypical viewpoint are the inversion motion of pyramidal molecules, e.g. ammonia, and the inter-conversion of chiral isomers where both are usually modeled by an effective double-well potential.^{15,16} In these cases, there are two molecular structures each represented by a well and separated by a finite potential barrier; however, the true ground state wavefunction is indeed a superposition of the wavefunctions of these two structures.

¹⁷⁻¹⁹ Evidently, in the superposed ground state certain, if not all, nuclei are “delocalized” in two (or sometimes more) spatial positions, and the simple picture of a “localized” nucleus excusing around an equilibrium spatial point is no longer applicable.

The question arises why such superposed states are not usually observable in chemical experiments. Various physical mechanisms, e.g. the environmentally induced decoherence,²⁰⁻²³ and certain mathematical constraints, e.g. the spontaneous symmetry breaking or the superselection rules,²⁴⁻²⁷ have been utilized to explain the subtlety of observation of such states. Nonetheless, currently, there is no doubt that it is experimentally feasible to construct such superposed states in a controllable way in sufficiently isolated situations.^{28,29}

One interesting example of such systems is the malonaldehyde molecule wherein the proton between the two oxygen atoms experiences an effective double-well potential.^{30,31} The two indistinguishable conformers, depicted in Figure 1, are local minima on the PES, with C_s geometrical symmetry, that are derivable from the electronic Schrödinger equation.³² The proton transfer reaction involves a transition state, depicted in Figure 1, with C_{2v} geometrical symmetry.³²⁻³⁴

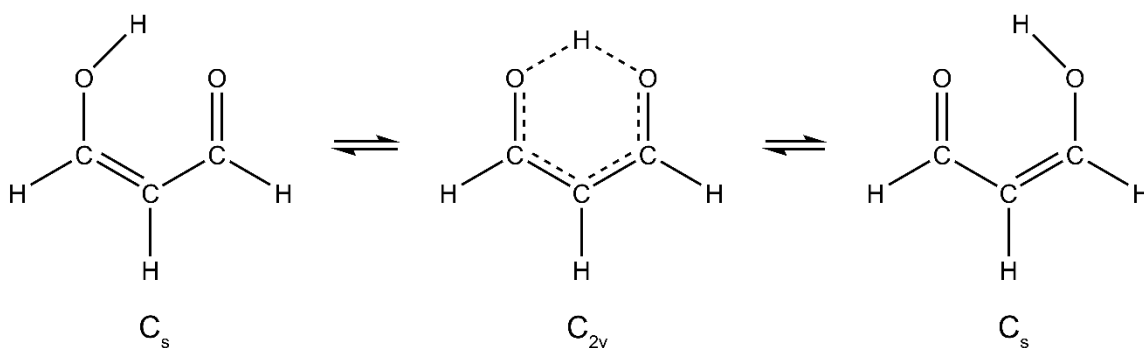


Figure 1 Schematic representation of the intra-molecular hydrogen transfer in malonaldehyde between the two conformers, C_s , passing through the transition state, C_{2v} .

The proton transfer between the two local minima may happen through the tunneling process, which has been extensively studied both theoretically,^{35–62} and experimentally,^{63–83} in the last decades. The tunneling mechanism implies that if **Cs** structures are prepared as stationary states, an oscillatory time-dependent non-stationary process must transform one conformer to the other.^{30,31} The alternative “delocalized” scenario emerges if the proton is treated as a quantum particle from the outset in the ab initio calculations. The resulting two-component Hamiltonian, which contains the kinetic energy operators of the proton and electrons simultaneously, belongs to the realm of the multi-component (MC) quantum chemistry.^{84–90} In that case, the resulting two-component (TC) wavefunctions of the ground and first excited states contain the electronic and protonic variables concurrently. If the MC Schrödinger equation is solved with sufficient accuracy,^{91–94} the probability densities of the proton’s wavefunctions in both states reveal two peaks at two distinct positions between the two oxygen atoms. These superposed structures are depicted schematically as **4**, the ground state, and **5**, the first excited state, in Figure 2 and compared to structures **1** to **3**. In the latter structures, the quantum proton is automatically confined to a spatial excursion around a reference point at the minima or the maximum on the effective PES depicted in Figure 2 and, these structures are the TC analogs of **Cs** and **C_{2v}**.

The molecular structures at their root are the networks of atoms in molecules (AIM) and their linking bonds. In line with this context, the quantum theory of atoms in molecules (QTAIM) is a quantum chemical partitioning methodology that divides a molecule exhaustively into atomic basins in the 3D real space and also partitions the molecular properties into the basin and inter-basin contributions.^{95–97} Since the QTAIM partitioning algorithm solely employs the electronic wavefunctions as the inputs to derive AIM and

their associated properties and interaction modes as the outputs, it fails to perform the AIM partitioning of the TC wavefunctions. To address this issue, the MC extension of the QTAIM, called MC-QTAIM, has recently been developed that is capable of partitioning the MC quantum systems by employing the ab initio MC wavefunctions.^{98–117} Our goal in this study is to decipher the molecular structures of the superposed states of malonaldehyde, **4** and **5**, by applying the MC-QTAIM to the corresponding wavefunctions.

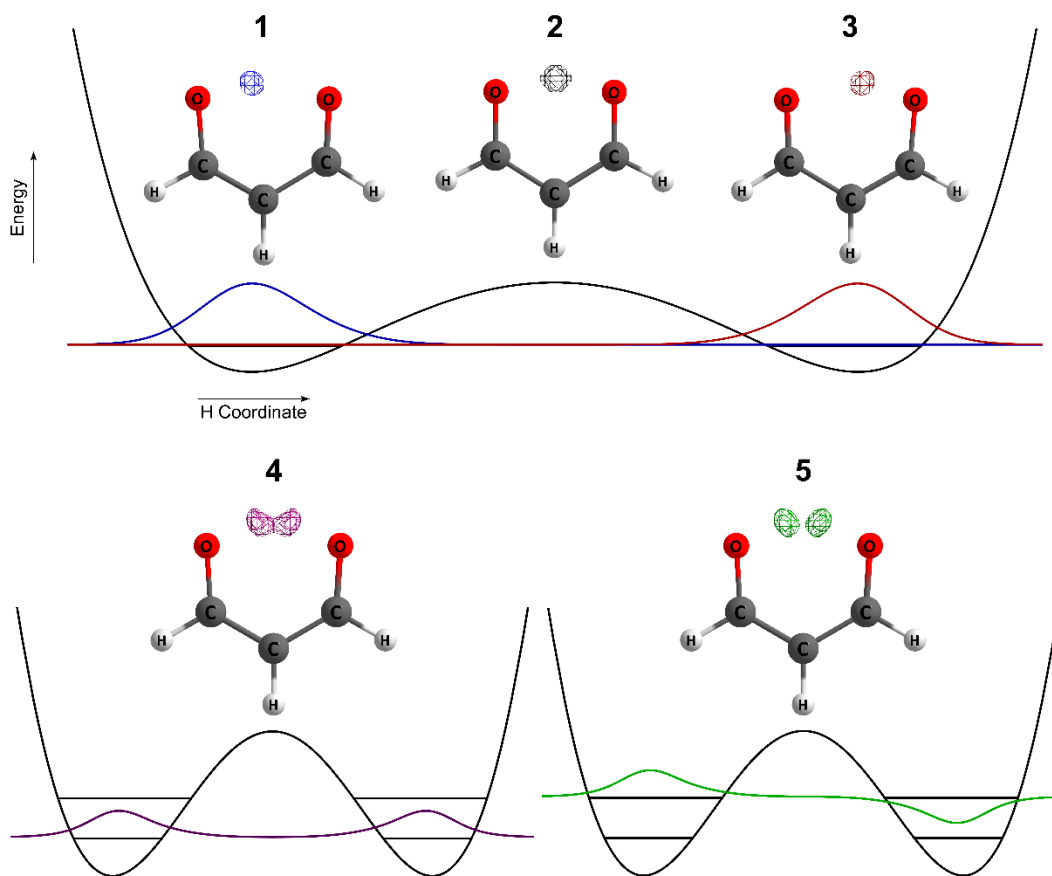


Figure 2 Schematic depictions of malonaldehyde structures with the localized (**1-3**) and delocalized protons (**4** and **5**), and, the corresponding one-dimensional cross section of the effective potential energy surfaces experienced by the proton along the axis connecting the two oxygen nuclei, denoted also by the H Coordinate, and the one-proton wavefunctions (while a single color has been used to depict the wavefunction of **5**, the phase of wavefunction is different in the two wells). The effective potential is the potential energy that is used in the one-particle Schrödinger equation governing the proton to deduce proton's wavefunction in a computational procedure detailed in the computational details section.

2. Theory and computational details

2.1. The MC-QTAIM

In the last decade, the QTAIM scheme has been extended to the partitioning of the MC quantum systems, and the input to the extended algorithm, called MC-QTAIM,^{98–117} are ab initio MC wavefunctions derived from solving the MC Schrödinger equation (written in atomic units):

$$\begin{aligned}
& \hat{H}_{MC} \Psi_{MC} \left(\left\{ \bar{x}_{1,1}, \dots, \bar{x}_{1,N_1} \right\}, \dots, \left\{ \bar{x}_{s,1}, \dots, \bar{x}_{s,N_s} \right\}; \left\{ \bar{R}_\alpha \right\} \right) \\
& = E_{MC} \left(\left\{ \bar{R}_\alpha \right\} \right) \Psi_{MC} \left(\left\{ \bar{x}_{1,1}, \dots, \bar{x}_{1,N_1} \right\}, \dots, \left\{ \bar{x}_{s,1}, \dots, \bar{x}_{s,N_s} \right\}; \left\{ \bar{R}_\alpha \right\} \right), \\
& \hat{H}_{MC} = \sum_n^s (-1/2m_n) \sum_i^{N_n} \nabla_{n,i}^2 + \sum_n^s \sum_i^{N_n} \sum_{j>i}^{N_n} \frac{q_n^2}{|\vec{r}_{n,i} - \vec{r}_{n,j}|} + \sum_n^s \sum_{m>n}^s \sum_i^{N_n} \sum_j^{N_m} \frac{q_n q_m}{|\vec{r}_{n,i} - \vec{r}_{m,j}|} + \sum_n^s \sum_i^{N_n} \sum_\alpha^Q \frac{Z_\alpha q_n}{|\vec{R}_\alpha - \vec{r}_{n,i}|}
\end{aligned} \tag{1}$$

This equation governs a system with s types of distinguishable quantum particles, with spin-spatial variables $\bar{x}_{n,i} = (\vec{r}_{n,i}, \sigma_{n,i})$ for the i -th particle of the n -th type, where there are N_n number of particles with charge, q_n , and mass, m_n , interacting via the Coulomb law with each other and the clamped nuclei; there are Q number of the latter carrying Z_α charge and placed at \vec{R}_α . The zero-flux equation of the MC-QTAIM partitioning algorithm, used to derive the boundaries of the atomic basins, is as follows:^{105,117}

$$\vec{\nabla} \Gamma^{(s)}(\vec{r}) \cdot \vec{n}(\vec{r}) = 0, \quad \Gamma^{(s)}(\vec{r}) = \sum_n^s (m_1/m_n) \rho_n(\vec{r}) \tag{2}$$

Wherein, $\rho_n(\vec{r}) = N_n \int d\bar{x}_{1,1} \dots \int d\bar{x}_{n-1,N_n} \int d\sigma_{n,1} \int d\bar{x}_{n,2} \dots \int d\bar{x}_{s,N_s} \Psi_{MC}^* \Psi_{MC}$ is the one-particle density of n -th type of particles.^{105,117} The Gamma density, $\Gamma^{(s)}$, which replaces the one-electron density used within the context of the QTAIM, is a mass-scaled combined density

that includes the contributions of all quantum particles in shaping the boundaries. The numbering of particle types relies on their mass and starts from the lightest to the heaviest particle type, e.g. for a system composed of electrons and protons as quantum particles, $\rho_1(\vec{r})$ and $\rho_2(\vec{r})$ are the electron and the proton one-densities, respectively. Some quantum particles, e.g. hydrogen isotopes, can form their own atomic basins, and the number of basins in an MC system is generally larger than the number of clamped nuclei, $P > Q$.^{107,108} The one-particle properties, $\hat{M} = \sum_n \hat{M}_n = \sum_n \left(\sum_i^{N_n} \hat{m}_{n,i} \right)$, are partitioned into

basin contributions as follows:^{104,105}

$$\langle \hat{M} \rangle = \left\langle \sum_n^s \sum_i^{N_n} \hat{m}_{n,i} \right\rangle = \sum_k^P \tilde{M}(\Omega_k), \quad \tilde{M}(\Omega_k) = \sum_n^s M_n(\Omega_k) \quad (3)$$

Wherein, $M_n(\Omega_k) = N_n \int d\vec{x}_{1,1} \dots \int d\vec{x}_{n-1,N_n} \int_{\Omega_k} d\vec{r}_{n,1} \int d\sigma_{n,1} \int d\vec{x}_{n,2} \dots \int d\vec{x}_{s,N_s} \text{Re} \left[\Psi_{MC}^* \hat{m}_{n,1} \Psi_{MC} \right]$

is the contribution of n -th type of particles to the basin property \hat{M} . In principle, the basin contribution originates from all types of particles though in practice some heavy particles are localized around a certain position and merely contribute to the properties of the basins within which they are confined.^{101,107-109,112} The partitioning of the two-particle

properties, $\hat{G} = \sum_n^s \left(\sum_i^{N_n} \sum_{j>i}^{N_n} \hat{g}_{n,ij} \right) + \sum_n^s \sum_{m>n}^s \left(\sum_i^{N_n} \sum_j^{N_m} \hat{g}_{nm,ij} \right)$, is done as follows:^{112,115,116}

$$\langle \hat{G} \rangle = \sum_k^P \tilde{G}(\Omega_k) + \sum_k^P \sum_{l>k}^P \tilde{G}(\Omega_k, \Omega_l),$$

$$\tilde{G}(\Omega_k) = \sum_n^s \left[G_n(\Omega_k) + \sum_{m>n}^s G_{nm}(\Omega_k) \right], \quad \tilde{G}(\Omega_k, \Omega_l) = \sum_n^s \left[G_n(\Omega_k, \Omega_l) + \sum_{m>n}^s G_{nm}(\Omega_k, \Omega_l) \right]$$

(4)

Wherein:

$$G_n(\Omega_k) = (N_n(N_n - 1)/2) \int_{\Omega_k} d\bar{x}_{1,1} \dots \int_{\Omega_k} d\bar{r}_{n,1} \int_{\Omega_k} d\sigma_{n,1} \int_{\Omega_k} d\bar{r}_{n,2} \int_{\Omega_k} d\sigma_{n,2} \dots \int_{\Omega_k} d\bar{x}_{s,N_s} \text{Re} \left[\Psi_{MC}^* \hat{g}_n(\bar{r}_1, \bar{r}_2) \Psi_{MC} \right]$$

$$G_{nm}(\Omega_k) = N_n N_m \int_{\Omega_k} d\bar{x}_{1,1} \dots \int_{\Omega_k} d\bar{r}_{n,1} \int_{\Omega_k} d\sigma_{n,1} \dots \int_{\Omega_k} d\bar{r}_{m,1} \int_{\Omega_k} d\sigma_{m,1} \dots \int_{\Omega_k} d\bar{x}_{s,N_s} \text{Re} \left[\Psi_{MC}^* \hat{g}_{nm}(\bar{r}_{n,1}, \bar{r}_{m,1}) \Psi_{MC} \right],$$

$$G_n(\Omega_k, \Omega_l) = (N_n(N_n - 1)/2) \int_{\Omega_k} d\bar{x}_{1,1} \dots \int_{\Omega_k} d\bar{r}_{n,1} \int_{\Omega_l} d\sigma_{n,1} \int_{\Omega_l} d\bar{r}_{n,2} \int_{\Omega_l} d\sigma_{n,2} \dots \int_{\Omega_l} d\bar{x}_{s,N_s} \text{Re} \left[\Psi_{MC}^* \hat{g}_n(\bar{r}_1, \bar{r}_2) \Psi_{MC} \right],$$

$$G_{nm}(\Omega_k, \Omega_l) = N_n N_m \int_{\Omega_k} d\bar{x}_{1,1} \dots \int_{\Omega_k} d\bar{r}_{n,1} \int_{\Omega_l} d\sigma_{n,1} \dots \int_{\Omega_l} d\bar{r}_{m,1} \int_{\Omega_l} d\sigma_{m,1} \dots \int_{\Omega_l} d\bar{x}_{s,N_s} \text{Re} \left[\Psi_{MC}^* \hat{g}_{nm}(\bar{r}_{n,1}, \bar{r}_{m,1}) \Psi_{MC} \right].$$

The prime application of this scheme is the extension of the interacting quantum atoms (IQA) energy partitioning scheme,^{118–122} to the MC systems through the partitioning of the inter-particle Coulomb interactions (vide infra).

The openness of the atomic basins with respect to the electron exchange is quantified within the context of the MC-QTAIM by introducing the basin particle number distributions, $P_m^n(\Omega_k)$, and then computing their mean, intra-basin variance and inter-basin covariance as follows:^{106,116,117}

$$P_m^n(\Omega_k) = \binom{N_n}{m} \int_{\Omega_k} d\bar{r}_{n,1} \dots \int_{\Omega_k} d\bar{r}_{n,m} \int_{R^3 - \Omega_k} d\bar{r}_{n,m+1} \dots \int_{R^3 - \Omega_k} d\bar{r}_{n,N_n} \prod_i^{N_n} \int d\sigma_{n,i} \int_{\Omega_k} d\bar{x}_{1,1} \dots \int_{\Omega_k} d\bar{x}_{n-1,N_{n-1}} \int_{\Omega_k} d\bar{x}_{n+1,1} \dots \int_{\Omega_k} d\bar{x}_{s,N_s} \Psi_{MC}^* \Psi_{MC}$$

$$N_n(\Omega_k) = \sum_m^{N_n} m P_m^n(\Omega_k) = \int_{\Omega_k} d\bar{r} \rho_n(\bar{r}),$$

$$Cov_n(\Omega_k, \Omega_l) = \int_{\Omega_k} d\bar{r}_1 \int_{\Omega_l} d\bar{r}_2 \rho_n^{(2)}(\bar{r}_1, \bar{r}_2) - N_n(\Omega_k) N_n(\Omega_l)$$

$$Var_n(\Omega_k) = \sum_m^{N_n} (m - N(\Omega_k))^2 P_m^n(\Omega_k) = \int_{\Omega_k} d\bar{r}_1 \int_{\Omega_k} d\bar{r}_2 \rho_n^{(2)}(\bar{r}_1, \bar{r}_2) + N_n(\Omega_k) - [N_n(\Omega_k)]^2$$

(5)

Wherein,

$\rho_n^{(2)}(\vec{r}_{n,1}, \vec{r}_{n,2}) = N_n(N_n - 1) \int d\vec{x}_{1,1} \dots \int d\vec{x}_{n-1, N_n} \int d\sigma_{n,1} \int d\sigma_{n,2} \int d\vec{x}_{n,3} \dots \int d\vec{x}_{s, N_s} \Psi_{MC}^* \Psi_{MC}$ is the spinless reduced second-order density matrix for the n -th type of particles.^{106,116,117} The basin particle number distribution is the probability distribution of observing m -particles from the n -th type within the k -th basin while the rest of $N_n - m$ particles are in the rest of the basins. The index of particle delocalization is introduced as follows: $\delta_n(\Omega_k, \Omega_l) = 2|Cov_n(\Omega_k, \Omega_l)|$, which is a gauge of the openness of an atomic basin with respect to the exchange of n -th type of particles with other basins.

The extended IQA method within the context of the MC-QTAIM was first developed and applied for the TC systems containing various isotopes of hydrogen as well as positronic systems using ab initio TC Hartree-Fock (TC-HF) wavefunctions.^{112,115} The details of the intra-basin terms may be found in the original references,^{112,115} but beyond the TC-HF approximation, for a fully correlated TC wavefunction the inter-basin terms of the extended IQA partitioning for a two-component (TC) system, composed of electrons and a proton, are as follows:

$$V_{elec}^{cl}(\Omega_k, \Omega_l) = V_{en}(\Omega_k, \Omega_l) + V_{en}(\Omega_l, \Omega_k) + V_{ee}^{cl}(\Omega_k, \Omega_l) + V_{nm}(\Omega_k, \Omega_l)$$

$$V_p^{cl}(\Omega_k, \Omega_l) = V_{ep}^{cl}(\Omega_k, \Omega_l) + V_{ep}^{cl}(\Omega_l, \Omega_k) + V_{pn}(\Omega_k, \Omega_l) + V_{pn}(\Omega_l, \Omega_k)$$

$$E_{inter}^{elec}(\Omega_k, \Omega_l) = V_{elec}^{cl}(\Omega_k, \Omega_l) + V_{elec}^{xc}(\Omega_k, \Omega_l)$$

$$E_{inter}^{total}(\Omega_k, \Omega_l) = E_{inter}^{elec}(\Omega_k, \Omega_l) + V_p^{cl}(\Omega_k, \Omega_l) + V_{ep}^c(\Omega_k, \Omega_l) + V_{ep}^c(\Omega_l, \Omega_k)$$

(6)

The details of each term are as follows:

$$\begin{aligned}
V_{en}(\Omega_k, \Omega_l) &= -Z_k \int_{\Omega_l} d\vec{r}_{1,1} \frac{\rho_1(\vec{r}_{1,1})}{|\vec{r}_{1,1} - \vec{R}_k|}, & V_{en}(\Omega_l, \Omega_k) &= -Z_l \int_{\Omega_k} d\vec{r}_{1,1} \frac{\rho_1(\vec{r}_{1,1})}{|\vec{r}_{1,1} - \vec{R}_l|}, \\
V_{ee}^{cl}(\Omega_k, \Omega_l) &= \int_{\Omega_k} d\vec{r}_{1,1} \int_{\Omega_l} d\vec{r}_{1,2} \frac{\rho_1(\vec{r}_{1,1})\rho_1(\vec{r}_{1,2})}{|\vec{r}_{1,1} - \vec{r}_{1,2}|}, & V_{elec}^{xc}(\Omega_k, \Omega_l) &= \int_{\Omega_k} d\vec{r}_{1,1} \int_{\Omega_l} d\vec{r}_{1,2} \frac{\rho_1^{xc}(\vec{r}_{1,1}, \vec{r}_{1,2})}{|\vec{r}_{1,1} - \vec{r}_{1,2}|} \\
V_{m}(\Omega_k, \Omega_l) &= \frac{Z_k Z_l}{|\vec{R}_k - \vec{R}_l|}, & V_{ep}^{cl}(\Omega_k, \Omega_l) &= - \int_{\Omega_k} d\vec{r}_{1,1} \int_{\Omega_l} d\vec{r}_{2,1} \frac{\rho_1(\vec{r}_{1,1})\rho_2(\vec{r}_{2,1})}{|\vec{r}_{1,1} - \vec{r}_{2,1}|} \\
V_{ep}^{cl}(\Omega_l, \Omega_k) &= - \int_{\Omega_l} d\vec{r}_{1,1} \int_{\Omega_k} d\vec{r}_{2,1} \frac{\rho_1(\vec{r}_{1,1})\rho_2(\vec{r}_{2,1})}{|\vec{r}_{1,1} - \vec{r}_{2,1}|}, & V_{pm}(\Omega_k, \Omega_l) &= Z_k \int_{\Omega_l} d\vec{r}_{2,1} \frac{\rho_2(\vec{r}_{2,1})}{|\vec{r}_{2,1} - \vec{R}_k|} \\
V_{pm}(\Omega_l, \Omega_k) &= Z_l \int_{\Omega_l} d\vec{r}_{2,1} \frac{\rho_2(\vec{r}_{2,1})}{|\vec{r}_{2,1} - \vec{R}_l|}, & V_{ep}^c(\Omega_k, \Omega_l) &= - \int_{\Omega_l} d\vec{r}_{1,1} \int_{\Omega_k} d\vec{r}_{2,1} \frac{\rho_{12}^c(\vec{r}_{1,1}, \vec{r}_{2,1})}{|\vec{r}_{1,1} - \vec{r}_{2,1}|}, \\
V_{ep}^c(\Omega_l, \Omega_k) &= - \int_{\Omega_l} d\vec{r}_{1,1} \int_{\Omega_k} d\vec{r}_{2,1} \frac{\rho_{12}^c(\vec{r}_{1,1}, \vec{r}_{2,1})}{|\vec{r}_{1,1} - \vec{r}_{2,1}|} & & (7)
\end{aligned}$$

In this partitioning scheme the spinless reduced second-order density matrix for electrons and the electron-proton pair density are decomposed as follows:

$$\rho_1^{(2)}(\vec{r}_{1,1}, \vec{r}_{1,2}) = \rho_1(\vec{r}_{1,1})\rho_1(\vec{r}_{1,2}) + \rho_1^{xc}(\vec{r}_{1,1}, \vec{r}_{1,2}), \quad \rho_{12}^{(2)}(\vec{r}_{1,1}, \vec{r}_{2,1}) = \rho_1(\vec{r}_{1,1})\rho_2(\vec{r}_{2,1}) + \rho_{12}^c(\vec{r}_{1,1}, \vec{r}_{2,1}),$$

respectively, where the pair density is defined as follows:

$$\rho_{12}^{(2)}(\vec{r}_{1,1}, \vec{r}_{2,1}) = N_1 N_2 \int d\sigma_{1,1} \int d\vec{x}_{1,2} \dots \int d\vec{x}_{1,N_1} \int d\sigma_{2,1} \int d\vec{x}_{2,2} \dots \int d\vec{x}_{2,N_2} \Psi_{TC}^* \Psi_{TC}.$$

Let us stress, as reviewed comprehensively in a recent paper,¹¹⁶ that the MC-QTAIM analysis can be performed on a large number of many-body quantum systems, containing both positively and negatively charged quantum particles, with varying masses, even when the interactions between particles are not solely of Coulombic nature.

2.2. Computational details

The computational scheme used for ab initio calculations in the present study is the Nuclear-Electronic Orbital (NEO) methodology developed by Hammes-Schiffer and coworkers in the last two decades.^{85,89,90} The NEO includes a number of ab initio methods developed within a hierarchical framework,^{89,90} similar to the usual hierarchical structure

of the ab initio electronic structure theory,^{5,6} which tries to solve the MC Schrödinger equation, eq. (1). The method used in the present study is the NEO density functional theory (NEO-DFT) which is basically a TC formulation of the Kohn-Sham (KS) equations of DFT.^{62,123–133} The TC-KS wavefunction is a product of the electronic Slater determinant and the protonic KS spin-orbital. The computational implementation of the NEO-DFT includes the SCF solution of the TC-KS equations using the KS potentials derived from the electron-electron and electron-proton functionals.^{130,131,133} All nuclei except the target proton, between the two oxygen atoms, are treated as clamped point charges.

In principle, if the proper electron-electron exchange-correlation and the electron-proton correlation functionals are employed, through simultaneous optimization of the geometry of clamped nuclei and the one-electron and the one-proton densities, the superposed states of malonaldehyde must be recovered. However, many studies revealed that this is not an achievable task with the currently available electron-proton correlation functionals.^{85,91,92} Instead, full optimization through the TC-KS equations yields “broken symmetry” KS wavefunctions that are basically describing structures **1** and **3**. Even more, in the whole toolkit of the ab initio MC quantum chemistry, only very accurate MC-full-configuration-interaction derived wavefunctions, or very high-quality MC-multi-configurational SCF wavefunctions, may recover the superposed states via full optimization.⁹¹ Such methodologies are beyond the current computational capacity for systems with a size around malonaldehyde. Inevitably, some computational tricks like the “geometry/state-averaging” must be used to first reach a symmetric geometry which would subsequently, be employed to derive the desired “delocalized” KS wavefunctions, as justified in some previous studies.^{58,94} Accordingly, in the first step, a geometry for

clamped nuclei in **4** and **5** was generated by the geometry-averaging method of the internal coordinates of the equilibrium geometries of **1** and **3**. The C_s and C_{2v} geometries of malonaldehyde, previously obtained by Hargis et al. at the CCSD(T)/cc-pVQZ level,³² were used for the geometry averaging procedure (see the Supporting information (SI) for details). In the averaging procedure, the arithmetic mean of the corresponding Z-matrix coordinates of **1** and **3** was computed after ordering the coordinates of the two Z-matrices. Let us stress the geometry averaging procedure is not unique however, the results of the MC-QTAIM analysis, as will be discussed subsequently, are not sensitive to the details of geometry as far as the geometrical variations relative to the one used in this study is not large.

To obtain the ground and first excited one-proton wavefunctions, i.e. structures **4** and **5**, respectively, the three-dimensional time-independent Schrödinger equation of the quantum proton was solved by the Numerov method in a cubic grid of 1.75 Å edge width, using 48 grid points per dimension; the used proton mass is 1836.153 in atomic units.⁶¹ The center of the cubic grid was placed at the point $(x,y,z) = (0.0, 0.0, 0.2)$ in the coordinate system used to represent the averaged structures, as given in the SI. The cubic grid spanned from -0.875 Å to 0.875 Å in x and y directions and from -0.675 Å to 1.075 Å in z direction covering the most critical spatial domain for the representation of the quantum proton's wavefunction. The corresponding electronic ground-state PES for the Numerov method was derived at MP2/cc-pVTZ level at each grid point assuming a clamped proton. The high efficiency and accuracy of the *improved* Numerov method in solving high dimensional differential equations have been recently demonstrated in considering the molecular vibrational modes.^{134–136} In the present study, we used the 7-point stencil that enabled us

to reach the accuracy $O(10^{-7})$ in the solution of the grid-based Numerov methodology. In addition, the JADAMILU eigenvalue problem library was employed for the diagonalization procedure that takes advantage of the highly-sparse representation of the Hamiltonian formed within the Numerov approach.¹³⁷ In the next step, each numerical grid of the proton's wavefunction was fitted to a set of 6s6p6d Gaussian functions, by full optimization of their coefficients, exponents and centers (see the SI for details). The fitted proton's wavefunction was then used as an initial guess for the protonic orbital in the SCF procedure of the NEO-DFT. The cyclic updates of the protonic density were avoided during the SCF procedure to obtain the optimized electronic part of the TC-KS wavefunction at B3LYP/[cc-pVTZ:6s6p6d] level.^{138,139} Accordingly, this approach could be seen as a frozen nuclear density approximation where the one-proton density remained unchanged during the optimization of the one-electron density.

Instead of the usual single-center expansion of the electronic basis functions, two sets of hydrogen cc-pVTZ basis set,¹³⁸ were placed at the two positions corresponding to the maxima of the one-proton densities (See Figure 3). Let us stress at this stage that the mentioned computational procedure has not been designed for accurately reproducing the energy gap between the ground and excited superposed protonic states, but to infer proper TC-KS wavefunctions for the MC-QTAIM analysis. Also, in contrast to the product nature of the KS wavefunction, the fact that the electronic part of the KS wavefunction is derived self-consistently under the direct influence of the one-proton density makes the whole procedure distinct from any adiabatic procedure that treats electrons' and proton's dynamics separately.

At the next stage, and for comparison purposes, the TC-KS wavefunctions for **1** to **3**, were obtained at the two-component B3LYP:EPC17-1/cc-pVTZ:10s10p10d level,¹³⁰ by employing the CCSD(T)/cc-pVQZ optimized geometries.³² The protonic KS spatial orbital in each of the structures **1** to **3** was expanded by [10s10p10d] uncontracted shells of even-tempered Gaussian basis functions, which are placed at the optimized position of the transferring proton and their exponents spanned the range of $2\sqrt{2}$ to 64. In addition, the cc-pVTZ basis set was used to expand the electronic KS orbitals employing the clamped proton position derived at the CCSD(T)/cc-pVQZ level as the center of the electronic basis set. The used even-tempered protonic basis set is flexible enough to capture the anharmonicity and anisotropy of the protonic orbital, as has been shown in several recent NEO-DFT studies.^{131,140} The recently developed EPC17-1 electron-proton correlation functional was used to produce high-quality one-proton density which is comparable to that derived from highly accurate ab-initio results of the MC coupled-cluster theory.^{130,141} The NEO methodology was originally implemented into the GAMESS quantum chemistry package although the computations reported in the this paper have been derived via our in-house version of the NEO-GAMESS package.^{85,123,142,143} Some details of the ab initio results are gathered in Table S1 in the SI.

The extended IQA partitioning of the electronic exchange-correlation energy of **1** to **5** was done according to the formalism discussed in the previous subsection and based on the IQA-DFT partitioning developed previously.^{144,145} Since no electron-proton correlation functional is used in the NEO-DFT calculations of **4** and **5**, the electron-proton correlation energy is zero and the total inter-basin interaction energy reduces to:

$$E_{\text{inter}}^{\text{total}}(\Omega_k, \Omega_l) = E_{\text{inter}}^{\text{elec}}(\Omega_k, \Omega_l) + V_p^{\text{cl}}(\Omega_k, \Omega_l).$$

The AIMALL package, T. A. Keith, AIMAll

(Version 13.11.04), TK Gristmill Software, Overland Park KS, USA, 2013, was used for the MC-QTAIM calculations including the graphics of the molecular graphs and the interatomic surfaces. All computational results are offered in the atomic units both in the main text and the SI.

3. Results and discussion

To start the MC-QTAIM analysis, the computed TC-KS wavefunctions were used to derive the one-electron, $\rho_1(\vec{r})$, and the one-proton, $\rho_2(\vec{r})$, densities as well as various energy partition terms of the extended IQA method. Figure 3 depicts the ab initio computed $\rho_2(\vec{r})$ revealing the expected “localized” nature of the one-proton density in **1** to **3** which is in marked contrast to its “delocalized” representation in **4** and **5**. At the next stage, the MC-QTAIM partitioning was performed by employing the Gamma density, $\Gamma^{(2)}(\vec{r}) = \rho_1(\vec{r}) + (1/m_{proton})\rho_2(\vec{r})$, and the results have been summarized in Figures 4 and 5. The topological analysis of $\vec{\nabla}\Gamma^{(2)}(\vec{r})$ in **1** to **3** yields the same number and types of critical points (CPs), and thus, provides the same types of AIM that were also previously deduced from the QTAIM analysis of the ab initio electronic wavefunction of **C_s** and **C_{2v}** structures.¹⁴⁶ In contrast, for the superposed states, **4** and **5**, the AIM structures are quite distinct and no hydrogen basin emerges between the two oxygen basins. It seems upon delocalization in two distinct spatial positions, the proton loses its capability to attract enough electrons and form its own maxima, i.e. (3, -3) CP in $\Gamma^{(2)}(\vec{r})$, and somehow “dissolves” in the two basins containing the clamped oxygen nuclei (for the nomenclature used to classify CPs see Bader’s monograph).⁹⁵ It seems that these exotic basins are better to be called the “hybrid oxygen-hydrogen” basins, hereafter denoted as *O4H* and *O5H*, to

make a distinction from the usual oxygen basins in **1** to **3**. In the previous studies, this phenomenon was observed only for the light positively-charged quantum particles, e.g. positrons.^{99,115}

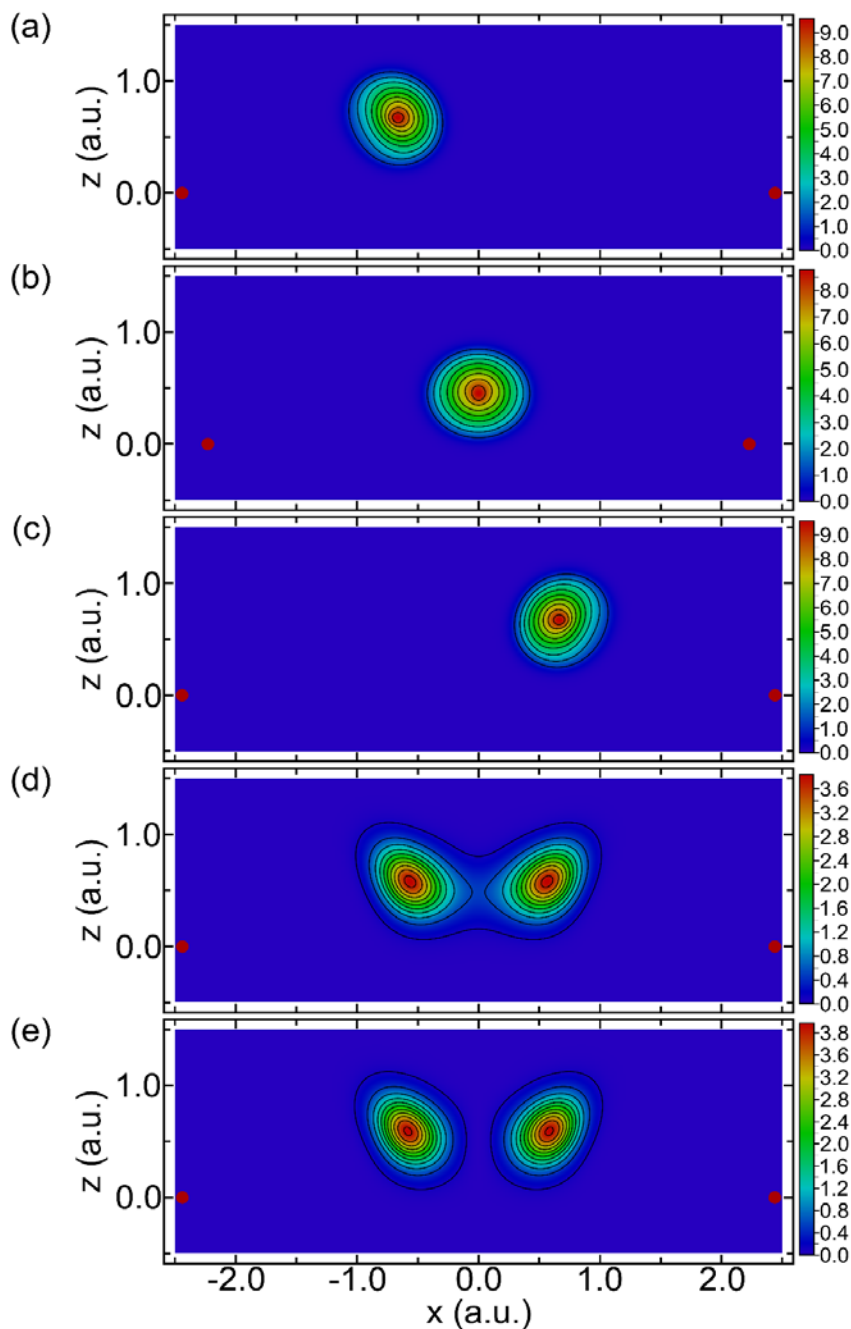


Figure 3 2D contour maps of the one-proton densities of (a) **1**, (b) **2**, (c) **3**, (d) **4** and (e) **5** structures. The positions of the clamped oxygen nuclei are depicted by red dots while the other nuclei are placed at the negative region of the z -axis on the xz plane (see Figure 2).

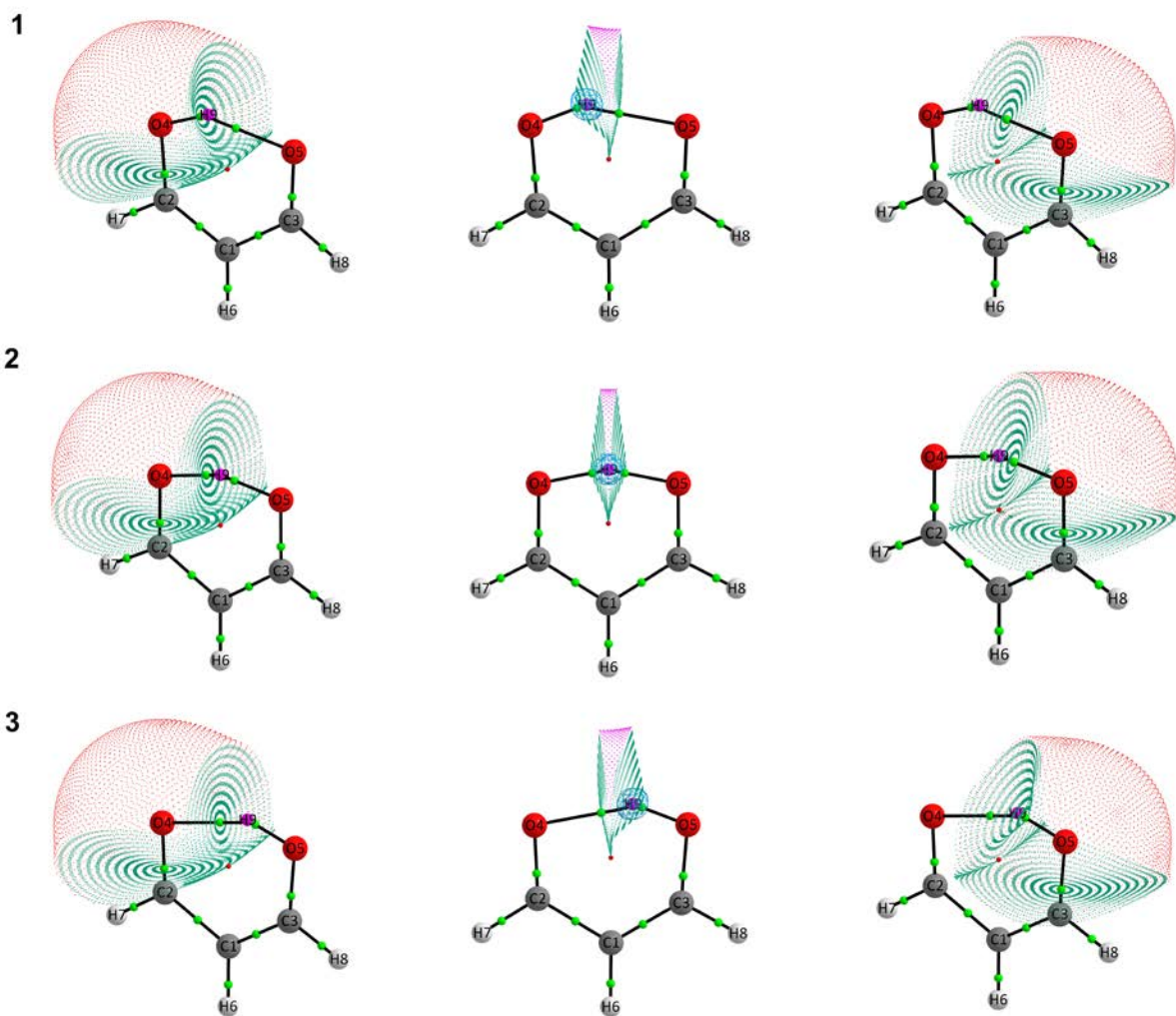
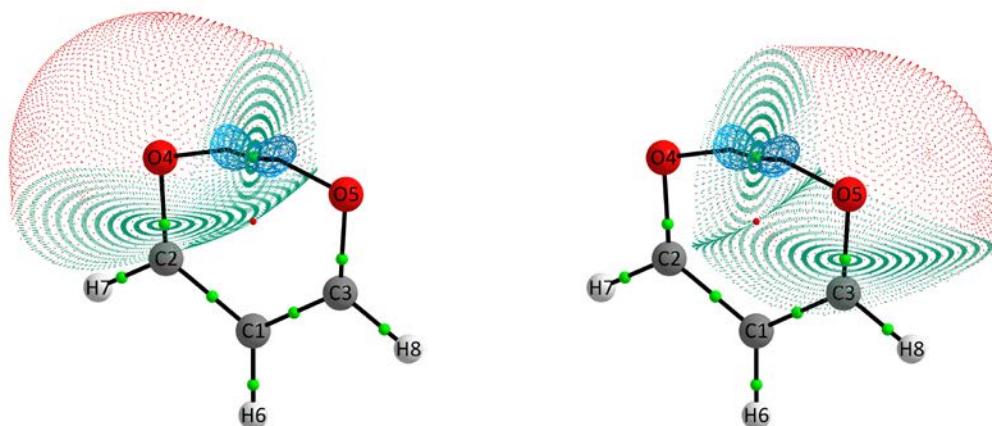


Figure 4 The AIM structures of **1** to **3**. The blue spherical mesh is the 3D iso-density surface of the proton one-density shown at 0.0001 a.u. (for a complementary view see Figure 3) while the purple, red, and green spheres are the (3, -3), (3, +1), and (3, -1) types CPs of $\Gamma^{(2)}(\vec{r})$, respectively. The black lines are the line paths and the green surfaces are the boundaries of oxygen and hydrogen basins. The red and purple meshes show surfaces where $\Gamma^{(2)}(\vec{r})$ equals 0.001 a.u. which are an arbitrary but reasonable outer boundaries for the oxygen and hydrogen basins, respectively. The (3, -3) nuclear attractors at (or very near to) the clamped nuclei are shown by the larger spheres and labeled according to their elemental constituents.

4



5

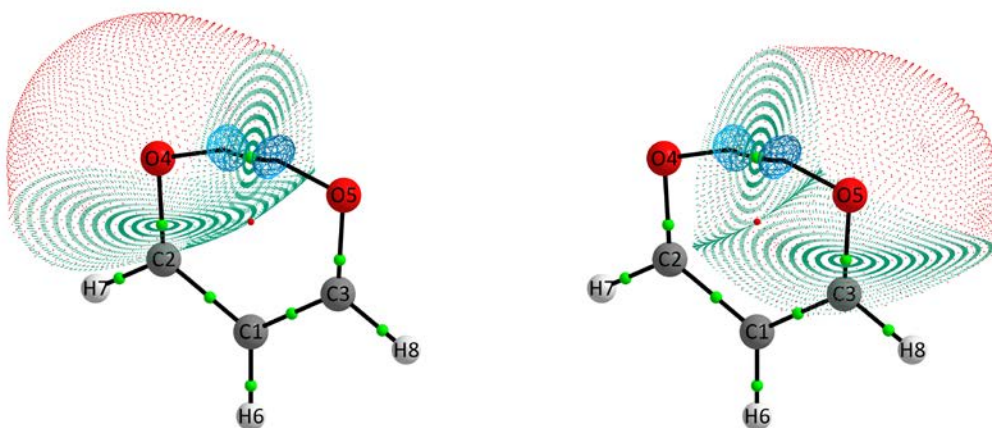


Figure 5 The AIM structures of **4** and **5**. The blue spherical mesh in each structure is the 3D iso-density surface of the proton one-density shown at 0.0001 a.u. (for a complementary view see Figure 3) while the red and green spheres are the (3, +1), and (3, -1) types CPs of $\Gamma^{(2)}(\vec{r})$, respectively. The black lines are the line paths and the green surfaces are the boundaries of the hybrid oxygen-hydrogen basins. The red mesh shows surfaces where $\Gamma^{(2)}(\vec{r})$ equals 0.001 a.u. which are an arbitrary but reasonable outer boundaries for the hybrid oxygen-hydrogen basins. The (3, -3) nuclear attractors at (or very near to) the clamped nuclei are shown by the larger spheres and labeled according to their elemental constituents.

Table 1 contains the atomic charges, $Q(A) = Z_{\Omega} - N_1(A) + N_2(A)$, of all basins and the electronic delocalization indices, $\delta_1(A, B)$,¹⁰⁶ between the neighboring basins, i.e. those sharing an inter-atomic boundary and a line critical point,¹⁴⁷ in **1** to **5**. The latter index is chemically interpretable as a measure of the covalent bond order.¹⁴⁸ The numerical values of $\delta_1(A, B)$ imply the expected covalent networks of bonds in **1** to **3**, which are practically indistinguishable from those depicted schematically in Figure 1. On the other hand, they reveal that the molecular structures of **4** and **5** are virtually the same, and the AIM structures and bonding networks of the backbones, i.e. all the basins except the two hybrid basins, as well as the bonding between the hybrid and neighboring carbon basins, are quite similar to that of **2**. So, what remains unclear at this stage is the nature of the interaction between the hybrid basins. To dig into the nature of hybrid basins' interactions, the extended IQA energy partitioning, was applied to **1** to **5**, and the computed two-particle inter-basin terms are considered herein. The results of the extended IQA partitioning of **1** to **3**, gathered in Table 2, conform fully to the nature of bonds derived from the values of $\delta_1(A, B)$ and they may be used as the reference to deduce the nature of bonds in **4** and **5**. Table 3 offers the results of the extended IQA analysis for **4** and **5** revealing the fact that they share quite similar bonding networks in the backbone. All the bonded basin pairs, except for the hybrid pair, have stabilizing inter-basin electronic interactions, $E_{\text{inter}}^{\text{elec}}(A, B) = V_{\text{elec}}^{\text{cl}}(A, B) + V_{\text{elec}}^{\text{xc}}(A, B)$, since the inter-basin electronic exchange-correlation interaction energies, $V_{\text{elec}}^{\text{xc}}(A, B)$, are always stabilizing. Adding the total inter-basin classical Coulomb interaction of electrons and clamped nuclei with the proton does

not change this picture and the total inter-basin interactions,

$E_{\text{inter}}^{\text{total}}(A, B) = E_{\text{inter}}^{\text{elec}}(A, B) + V_p^{\text{cl}}(A, B)$, are also always stabilizing.

Table 1 The atomic charges and electronic delocalization index ($\delta_1(A, B)$) of species **1** to **5** (see Figure 4 for the numbering of the atomic basins).*

<i>Atomic basin</i>	3 (=1)	2	<i>Atomic basin</i>	3 (=1)	2
	<i>charge</i>	<i>charge</i>		$\delta_1(A, B)$	$\delta_1(A, B)$
C1	-0.02	-0.04			
C2	0.94	0.78	C1	1.14	1.32
C3	0.61	0.78	C1	1.51	1.32
O4	-1.14	-1.15	C2	1.34	1.19
O5	-1.20	-1.15	C3	1.05	1.19
H6	0.03	0.04	C1	0.96	0.97
H7	0.02	0.05	C2	0.90	0.91
H8	0.06	0.05	C3	0.92	0.91
H9	0.69	0.67	O5/O4	0.40/0.11	0.28
	4	5		4	5
C1	-0.05	-0.05			
C2	0.78	0.78	C1	1.32	1.32
C3	0.78	0.78	C1	1.32	1.32
H6	0.03	0.03	C1	0.97	0.97
H7	0.04	0.04	C2	0.91	0.91
H8	0.04	0.04	C3	0.91	0.91
O4H	-0.82	-0.82	C2	1.20	1.20
O5H	-0.82	-0.82	O4H	0.29	0.28

Table 2 The selected results of the extended IQA energy partitioning for **1** to **3** (see Figure 4 for the numbering of the atomic basins).

		3 (=1)		
<i>Atomic basin</i>	<i>Atomic basin</i>	V_{elec}^{xc}	V_{elec}^{cl}	E_{inter}^{elec}
C1	C3	-0.446	0.064	-0.382
C2	C1	-0.352	0.049	-0.304
C3	O5	-0.316	-0.510	-0.826
H6	C1	-0.285	0.038	-0.247
H7	C2	-0.269	0.059	-0.211
H8	C3	-0.277	0.061	-0.216
O4	C2	-0.396	-0.722	-1.118
H9	O5	-0.127	0.159	0.032
H9	O4	-0.027	0.111	0.084
		2		
C1	C2/C3	-0.399	0.056	-0.343
C3	O5	-0.356	-0.612	-0.968
H6	C1	-0.287	0.038	-0.249
H7	C2	-0.274	0.063	-0.211
H8	C3	-0.274	0.063	-0.211
O4	C2	-0.356	-0.612	-0.968
H9	O5/O4	-0.084	0.154	0.069

Table 3 The selected results of the extended IQA energy partitioning for **4** and **5** (see Figure 5 for the numbering of the atomic basins).

4						
<i>Atomic basin</i>	<i>Atomic basin</i>	V_{elec}^{xc}	V_{elec}^{cl}	E_{inter}^{elec}	V_p^{cl}	E_{inter}^{total}
C1	C3	-0.398	0.053	-0.345	0.000	-0.345
C2	C1	-0.398	0.053	-0.345	0.000	-0.345
C3	O5	-0.358	-0.655	-1.013	0.145	-0.868
H6	C1	-0.286	0.037	-0.249	0.000	-0.249
H7	C2	-0.274	0.062	-0.212	0.000	-0.212
H8	C3	-0.274	0.062	-0.212	0.000	-0.212
O4H	C2	-0.358	-0.654	-1.012	0.145	-0.867
O5H	O4H	-0.055	0.425	0.370	-0.508	-0.138
5						
C1	C3	-0.398	0.053	-0.345	0.000	-0.345
C2	C1	-0.398	0.053	-0.345	0.000	-0.345
C3	O5	-0.358	-0.655	-1.013	0.147	-0.866
H6	C1	-0.286	0.037	-0.249	0.000	-0.249
H7	C2	-0.274	0.062	-0.212	0.000	-0.212
H8	C3	-0.274	0.062	-0.212	0.000	-0.212
O4H	C2	-0.358	-0.654	-1.012	0.147	-0.866
O5H	O4H	-0.053	0.423	0.370	-0.495	-0.124

In the case of the hybrid pair the inter-basin electronic exchange-correlation energy, $V_{elec}^{xc}(\Omega_{O4H}, \Omega_{O5H})$, slightly stabilizing but its absolute value is very small and negligible. Whereas, the inter-basin electronic classical Coulomb interaction energy, $V_{elec}^{cl}(\Omega_{O4H}, \Omega_{O5H})$, is largely destabilizing thus, the sole source of stabilizing interaction is $V_p^{cl}(\Omega_{O4H}, \Omega_{O5H})$. The latter term itself is composed of the destabilizing interaction between the proton and the oxygen nuclei, $V_{pn}(\Omega_{O4H}, \Omega_{O5H}) + V_{pn}(\Omega_{O5H}, \Omega_{O4H})$, and the stabilizing classical Coulomb interaction energy of the one-proton density in one of the basins with the one-electron density in the other basin, $V_{ep}^{cl}(\Omega_{O4H}, \Omega_{O5H}) + V_{ep}^{cl}(\Omega_{O5H}, \Omega_{O4H})$. Thus, the very origin of the stabilizing interaction between the hybrid basins is the latter terms in $V_p^{cl}(\Omega_{O4H}, \Omega_{O5H})$, and it seems reasonable to claim that these terms yield an unconventional chemical bond between the two hybrid basins. Let us stress that this mechanism of bonding is unprecedented in usual molecules but it is interestingly quite similar to the mechanism of formation of the newly proposed “positronic bond”.^{115,149}

4. Conclusion

Malonaldehyde is usually conceived as a typical organic molecule with a molecular structure consisted of a network of well-known C-C, C-O, C-H and O-H covalent bonds, and an intra-molecular resonant-assisted hydrogen bond.¹⁵⁰ Even susceptibility to the tunneling mechanism does not change this picture profoundly and adds an extra dynamical, time-dependent, aspect to its molecular structure.⁷⁶ However as demonstrated in the present study, applying the quantum superposition principle to the proton between the oxygen atoms alters significantly its molecular structure. In fact, the very basic and probably trivial

idea that each atom is a node in the molecular graph is called into question in the quantum superposed states, at least within the context of the present MC-QTAIM analysis. Evidently, a proper symbolic representation of molecular structures attributable to such exotic states is lacking in the current state of affairs and needs novel conventions and nomenclature. Probably, the fruitfulness of attributing molecular structures to such exotic states may be evaluated if the corresponding “exotic chemistry” will be amenable to future experimental studies. Indeed, the analysis of the AIM structure and the bonding network of the superposed nuclear states is a completely uncharted territory that awaits further theoretical and experimental developments and computational analysis.

Acknowledgments

The authors are grateful to Cina Foroutan-Nejad for his constructive comments.

References

- 1 J. Audretsch, *Entangled Systems: New Directions in Quantum Physics*, Wiley-VCH, Weinheim, 1st edition., 2007.
- 2 M. P. Silverman, *Quantum Superposition*, Springer, 2008.
- 3 T. A. Albright, J. K. Burdett and M.-H. Whangbo, *Orbital Interactions in Chemistry*, Wiley-Interscience, Hoboken, New Jersey, 2nd edition., 2013.
- 4 I. Fleming, *Molecular Orbitals and Organic Chemical Reactions*, Wiley, Chichester, West Sussex, U.K., Student edition., 2009.
- 5 A. Szabo and N. S. Ostlund, *Modern Quantum Chemistry: Introduction to Advanced Electronic Structure Theory*, Dover Publications, Mineola, N.Y, Reprint Edition., 1996.
- 6 T. Helgaker, P. Jørgensen and J. Olsen, *Molecular Electronic-Structure Theory*, John Wiley & Sons, Ltd, Chichester, UK, 2000.
- 7 H. Mustroph, Potential-Energy Surfaces, the Born–Oppenheimer Approximations, and the Franck–Condon Principle: Back to the Roots, *ChemPhysChem*, 2016, **17**, 2616–2629.
- 8 B. T. Sutcliffe and R. G. Woolley, Comment on ‘Molecular structure in non-Born–Oppenheimer quantum mechanics,’ *Chem. Phys. Lett.*, 2005, **408**, 445–447.
- 9 B. T. Sutcliffe and R. G. Woolley, Molecular structure calculations without clamping the nuclei, *Phys. Chem. Chem. Phys.*, 2005, **7**, 3664–3676.
- 10 A. G. Császár, C. Fábri, T. Szidarovszky, E. Mátyus, T. Furtenbacher and G. Czakó, The fourth age of quantum chemistry: molecules in motion, *Phys. Chem. Chem. Phys.*, 2012, **14**, 1085–1106.

- 11 R. G. Woolley, Quantum theory and molecular structure, *Adv. Phys.*, 1976, **25**, 27–52.
- 12 H. Primas, *Chemistry, Quantum Mechanics and Reductionism: Perspectives in Theoretical Chemistry*, Springer Berlin Heidelberg, Berlin, Heidelberg, 1983.
- 13 R. G. Woolley, The molecular structure conundrum, *J. Chem. Educ.*, 1985, **62**, 1082–1084.
- 14 A. Amann, Must a molecule have a shape?, *South Afr. J. Chem.*, 1992, **45**, 29–38.
- 15 Y. A. Berlin, A. L. Burin and V. V. Goldanskii, The Hund paradox and stabilization of molecular chiral states, *Z. Für Phys. At. Mol. Clust.*, 1996, **37**, 333–339.
- 16 C. Presilla, G. Jona-Lasinio and C. Toninelli, in *Multiscale Methods in Quantum Mechanics*, eds. P. Blanchard and G. Dell’Antonio, Birkhäuser, Boston, MA, 2004, pp. 119–127.
- 17 P. Claverie and G. Jona-Lasinio, Instability of tunneling and the concept of molecular structure in quantum mechanics: The case of pyramidal molecules and the enantiomer problem, *Phys. Rev. A*, 1986, **33**, 2245–2253.
- 18 B. R. Fischer and P. Mittelstaedt, Chirality as a quasi-classical property of molecular systems, *Phys. Lett. A*, 1990, **147**, 411–416.
- 19 J. A. Cina and R. A. Harris, Superpositions of Handed Wave Functions, *Science*, 1995, **267**, 832–833.
- 20 G. Jona-Lasinio, C. Presilla and C. Toninelli, Interaction Induced Localization in a Gas of Pyramidal Molecules, *Phys. Rev. Lett.*, 2002, **88**, 123001.
- 21 I. M. Herbauts and D. J. Dunstan, Quantum molecular dynamics study of the pressure dependence of the ammonia inversion transition, *Phys. Rev. A*, 2007, **76**, 062506.
- 22 M. A. Schlosshauer, *Decoherence and the Quantum-to-Classical Transition*, Springer, Berlin ; London, 2008.
- 23 J. Trost and K. Hornberger, Hund’s Paradox and the Collisional Stabilization of Chiral Molecules, *Phys. Rev. Lett.*, 2009, **103**, 023202.
- 24 U. Muller-Herold, A simple derivation of chemically important classical observables and superselection rules, *J. Chem. Educ.*, 1985, **62**, 379–382.
- 25 A. S. Wightman and N. Glance, Superselection rules in molecules, *Nucl. Phys. B - Proc. Suppl.*, 1989, **6**, 202–206.
- 26 G. Jona-Lasinio, Spontaneous Symmetry Breaking: Variations on a Theme, *Prog. Theor. Phys.*, 2010, **124**, 731–746.
- 27 C. Presilla and G. Jona-Lasinio, Spontaneous symmetry breaking and inversion-line spectroscopy in gas mixtures, *Phys. Rev. A*, 2015, **91**, 022709.
- 28 J. A. Cina and R. A. Harris, On the preparation and measurement of superpositions of chiral amplitudes, *J. Chem. Phys.*, 1994, **100**, 2531–2536.
- 29 C. Monroe, D. M. Meekhof, B. E. King and D. J. Wineland, A “Schrödinger Cat” Superposition State of an Atom, *Science*, 1996, **272**, 1131–1136.
- 30 F. Fillaux and B. Nicolai, Proton transfer in malonaldehyde: From reaction path to Schrödinger’s Cat, *Chem. Phys. Lett.*, 2005, **415**, 357–361.
- 31 F. Fillaux, A. Cousson and M. J. Gutmann, Proton transfer across hydrogen bonds: From reaction path to Schrödinger’s cat, *Pure Appl. Chem.*, 2007, **79**, 1023–1039.
- 32 J. C. Hargis, F. A. Evangelista, J. B. Ingels and H. F. Schaefer, Short Intramolecular Hydrogen Bonds: Derivatives of Malonaldehyde with Symmetrical Substituents, *J. Am. Chem. Soc.*, 2008, **130**, 17471–17478.

- 33 J. R. De La Vega, Role of symmetry in the tunneling of the proton in double-minimum potentials, *Acc. Chem. Res.*, 1982, **15**, 185–191.
- 34 T. Carrington and W. H. Miller, Reaction surface description of intramolecular hydrogen atom transfer in malonaldehyde, *J. Chem. Phys.*, 1986, **84**, 4364–4370.
- 35 E. M. Fluder and J. R. De la Vega, Intramolecular hydrogen tunneling in malonaldehyde, *J. Am. Chem. Soc.*, 1978, **100**, 5265–5267.
- 36 N. Shida, P. F. Barbara and J. E. Almlöf, A theoretical study of multidimensional nuclear tunneling in malonaldehyde, *J. Chem. Phys.*, 1989, **91**, 4061–4072.
- 37 N. Shida, J. Almlöf and P. F. Barbara, Tunneling paths in intramolecular proton transfer, *J. Phys. Chem.*, 1991, **95**, 10457–10464.
- 38 K. Luth and S. Scheiner, Excited-State Energetics and Proton-Transfer Barriers in Malonaldehyde, *J. Phys. Chem.*, 1994, **98**, 3582–3587.
- 39 V. A. Benderskii, E. V. Vetoshkin, I. S. Irgibaeva and H.-P. Trommsdorff, Multidimensional tunneling dynamics of proton transfer in malonaldehyde molecule and its isotopomers, *Russ. Chem. Bull.*, 2001, **50**, 1148–1158.
- 40 T. D. Sewell, Y. Guo and D. L. Thompson, Semiclassical calculations of tunneling splitting in malonaldehyde, *J. Chem. Phys.*, 1995, **103**, 8557–8565.
- 41 Z. Smedarchina, W. Siebrand and M. Z. Zgierski, An instanton approach to intramolecular hydrogen exchange: Tunneling splittings in malonaldehyde and the hydrogenoxalate anion, *J. Chem. Phys.*, 1995, **103**, 5326–5334.
- 42 K. Wolf, W. Mikenda, E. Nusterer and K. Schwarz, Proton motion in malonaldehyde: an ab initio molecular dynamics study, *J. Mol. Struct.*, 1998, **448**, 201–207.
- 43 M. Ben-Nun and T. J. Martínez, Semiclassical Tunneling Rates from Ab Initio Molecular Dynamics, *J. Phys. Chem. A*, 1999, **103**, 6055–6059.
- 44 V. A. Benderskii, E. V. Vetoshkin, I. S. Irgibaeva and H. P. Trommsdorff, Tunneling splittings in vibrational spectra of non-rigid molecules: IX. Malonaldehyde and its isotopomers as a test case for fully coupled multidimensional tunneling dynamics, *Chem. Phys.*, 2000, **262**, 393–422.
- 45 M. E. Tuckerman and D. Marx, Heavy-Atom Skeleton Quantization and Proton Tunneling in “Intermediate-Barrier” Hydrogen Bonds, *Phys. Rev. Lett.*, 2001, **86**, 4946–4949.
- 46 K. Yagi, T. Taketsugu and K. Hirao, Generation of full-dimensional potential energy surface of intramolecular hydrogen atom transfer in malonaldehyde and tunneling dynamics, *J. Chem. Phys.*, 2001, **115**, 10647–10655.
- 47 C. S. Tautermann, A. F. Voegelé, T. Loerting and K. R. Liedl, The optimal tunneling path for the proton transfer in malonaldehyde, *J. Chem. Phys.*, 2002, **117**, 1962–1966.
- 48 D. Babić, S. D. Bosanac and N. Došlić, Proton transfer in malonaldehyde: a model three-dimensional study, *Chem. Phys. Lett.*, 2002, **358**, 337–343.
- 49 G. V. Mil’nikov, K. Yagi, T. Taketsugu, H. Nakamura and K. Hirao, Tunneling splitting in polyatomic molecules: Application to malonaldehyde, *J. Chem. Phys.*, 2003, **119**, 10–13.
- 50 G. Kovačević, T. Hrenar and N. Došlić, Hydrogen bonding in malonaldehyde: a density functional and reparametrized semiempirical approach, *Chem. Phys.*, 2003, **293**, 41–52.

- 51 K. Yagi, G. V. Mil'nikov, T. Taketsugu, K. Hirao and H. Nakamura, Effect of out-of-plane vibration on the hydrogen atom transfer reaction in malonaldehyde, *Chem. Phys. Lett.*, 2004, **397**, 435–440.
- 52 M. D. Coutinho-Neto, A. Viel and U. Manthe, The ground state tunneling splitting of malonaldehyde: Accurate full dimensional quantum dynamics calculations, *J. Chem. Phys.*, 2004, **121**, 9207–9210.
- 53 K. Giese, M. Petković, H. Naundorf and O. Kühn, Multidimensional quantum dynamics and infrared spectroscopy of hydrogen bonds, *Phys. Rep.*, 2006, **430**, 211–276.
- 54 D. P. Tew, N. C. Handy and S. Carter, A reaction surface Hamiltonian study of malonaldehyde, *J. Chem. Phys.*, 2006, **125**, 084313.
- 55 A. Viel, M. D. Coutinho-Neto and U. Manthe, The ground state tunneling splitting and the zero point energy of malonaldehyde: A quantum Monte Carlo determination, *J. Chem. Phys.*, 2007, **126**, 024308.
- 56 P. P. Schmidt, The intramolecular tunnelling of hydrogen, *Mol. Phys.*, 2007, **105**, 1217–1237.
- 57 Y. Wang, B. J. Braams, J. M. Bowman, S. Carter and D. P. Tew, Full-dimensional quantum calculations of ground-state tunneling splitting of malonaldehyde using an accurate ab initio potential energy surface, *J. Chem. Phys.*, 2008, **128**, 224314.
- 58 A. Hazra, J. H. Skone and S. Hammes-Schiffer, Combining the nuclear-electronic orbital approach with vibronic coupling theory: Calculation of the tunneling splitting for malonaldehyde, *J. Chem. Phys.*, 2009, **130**, 054108.
- 59 M. Schröder, F. Gatti and H.-D. Meyer, Theoretical studies of the tunneling splitting of malonaldehyde using the multiconfiguration time-dependent Hartree approach, *J. Chem. Phys.*, 2011, **134**, 234307.
- 60 A. Yamada, H. Kojima and S. Okazaki, A molecular dynamics study of intramolecular proton transfer reaction of malonaldehyde in solutions based upon mixed quantum-classical approximation. I. Proton transfer reaction in water, *J. Chem. Phys.*, 2014, **141**, 084509.
- 61 U. Kuenzer, J.-A. Sorarù and T. S. Hofer, Pushing the limit for the grid-based treatment of Schrödinger's equation: a sparse Numerov approach for one, two and three dimensional quantum problems, *Phys. Chem. Chem. Phys.*, 2016, **18**, 31521–31533.
- 62 Z. Tao, Q. Yu, S. Roy and S. Hammes-Schiffer, Direct Dynamics with Nuclear–Electronic Orbital Density Functional Theory, *Acc. Chem. Res.*, 2021, **54**, 4131–4141.
- 63 W. F. Rowe, R. W. Duerst and E. B. Wilson, The intramolecular hydrogen bond in malonaldehyde, *J. Am. Chem. Soc.*, 1976, **98**, 4021–4023.
- 64 R. S. Brown, The intramolecular hydrogen bond in malonaldehyde as determined by x-ray photoelectron spectroscopy, *J. Am. Chem. Soc.*, 1977, **99**, 5497–5499.
- 65 S. L. Baughcum, R. W. Duerst, W. F. Rowe, Z. Smith and E. B. Wilson, Microwave spectroscopic study of malonaldehyde (3-hydroxy-2-propenal). 2. Structure, dipole moment, and tunneling, *J. Am. Chem. Soc.*, 1981, **103**, 6296–6303.
- 66 Z. Smith, E. B. Wilson and R. W. Duerst, The infrared spectrum of gaseous malonaldehyde (3-hydroxy-2-propenal), *Spectrochim. Acta Part Mol. Spectrosc.*, 1983, **39**, 1117–1129.

- 67 S. L. Baughcum, Z. Smith, E. B. Wilson and R. W. Duerst, Microwave spectroscopic study of malonaldehyde. 3. Vibration-rotation interaction and one-dimensional model for proton tunneling, *J. Am. Chem. Soc.*, 1984, **106**, 2260–2265.
- 68 P. Turner, S. L. Baughcum, S. L. Coy and Z. Smith, Microwave spectroscopic study of malonaldehyde. 4. Vibration-rotation interaction in parent species, *J. Am. Chem. Soc.*, 1984, **106**, 2265–2267.
- 69 G. Gilli, F. Bellucci, V. Ferretti and V. Bertolasi, Evidence for resonance-assisted hydrogen bonding from crystal-structure correlations on the enol form of the .beta.-diketone fragment, *J. Am. Chem. Soc.*, 1989, **111**, 1023–1028.
- 70 D. W. Firth, K. Beyer, M. A. Dvorak, S. W. Reeve, A. Grushow and K. R. Leopold, Tunable far-infrared spectroscopy of malonaldehyde, *J. Chem. Phys.*, 1991, **94**, 1812–1819.
- 71 T. Chiavassa, P. Roubin, L. Pizzala, P. Verlaque, A. Allouche and F. Marinelli, Experimental and theoretical studies of malonaldehyde: vibrational analysis of a strongly intramolecularly hydrogen bonded compound, *J. Phys. Chem.*, 1992, **96**, 10659–10665.
- 72 T. Baba, T. Tanaka, I. Morino, K. M. T. Yamada and K. Tanaka, Detection of the tunneling-rotation transitions of malonaldehyde in the submillimeter-wave region, *J. Chem. Phys.*, 1999, **110**, 4131–4133.
- 73 P. A. Cox, K. H. Hughes and J. N. MacDonald, Torsion—rotation interactions in monodeuterated acetaldehyde, *Mol. Phys.*, 2003, **101**, 569–574.
- 74 A. Alparone and S. Millefiori, Anharmonic vibrational spectroscopic investigation of malonaldehyde, *Chem. Phys.*, 2003, **290**, 15–25.
- 75 R. Srinivasan, J. S. Feenstra, S. T. Park, S. Xu and A. H. Zewail, Direct Determination of Hydrogen-Bonded Structures in Resonant and Tautomeric Reactions Using Ultrafast Electron Diffraction, *J. Am. Chem. Soc.*, 2004, **126**, 2266–2267.
- 76 H. Sekiya, in *Atom Tunneling Phenomena in Physics, Chemistry and Biology*, ed. T. Miyazaki, Springer, Berlin, Heidelberg, 2004, pp. 201–231.
- 77 C. Duan and D. Luckhaus, High resolution IR-diode laser jet spectroscopy of malonaldehyde, *Chem. Phys. Lett.*, 2004, **391**, 129–133.
- 78 Y. Arasaki, K. Yamazaki, M. T. do N. Varella and K. Takatsuka, Real-time observation of ground state proton transfer: a model study, *Chem. Phys.*, 2005, **311**, 255–268.
- 79 R. Meyer and T.-K. Ha, Rotational constants of malonaldehyde and isotopic species derived from ab initio results, *Mol. Phys.*, 2005, **103**, 2687–2698.
- 80 W. Caminati and J.-U. Grabow, The C_{2v} Structure of Enolic Acetylacetone, *J. Am. Chem. Soc.*, 2006, **128**, 854–857.
- 81 T. N. Wassermann, D. Luckhaus, S. Coussan and M. A. Suhm, Proton tunneling estimates for malonaldehyde vibrations from supersonic jet and matrix quenching experiments, *Phys. Chem. Chem. Phys.*, 2006, **8**, 2344–2348.
- 82 N. O. B. Lüttschwager, T. N. Wassermann, S. Coussan and M. A. Suhm, Vibrational tuning of the Hydrogen transfer in malonaldehyde – a combined FTIR and Raman jet study†, *Mol. Phys.*, 2013, **111**, 2211–2227.
- 83 W. Siebrand, Z. Smedarchina and A. Fernández-Ramos, Communication: Selection rules for tunneling splitting of vibrationally excited levels, *J. Chem. Phys.*, 2013, **139**, 021101.

- 84 M. Tachikawa, K. Mori, H. Nakai and K. Iguchi, An extension of ab initio molecular orbital theory to nuclear motion, *Chem. Phys. Lett.*, 1998, **290**, 437–442.
- 85 S. P. Webb, T. Iordanov and S. Hammes-Schiffer, Multiconfigurational nuclear-electronic orbital approach: Incorporation of nuclear quantum effects in electronic structure calculations, *J. Chem. Phys.*, 2002, **117**, 4106–4118.
- 86 H. Nakai, Nuclear orbital plus molecular orbital theory: Simultaneous determination of nuclear and electronic wave functions without Born–Oppenheimer approximation, *Int. J. Quantum Chem.*, 2007, **107**, 2849–2869.
- 87 T. Ishimoto, M. Tachikawa and U. Nagashima, Review of multicomponent molecular orbital method for direct treatment of nuclear quantum effect, *Int. J. Quantum Chem.*, 2009, **109**, 2677–2694.
- 88 A. Reyes, F. Moncada and J. Charry, The any particle molecular orbital approach: A short review of the theory and applications, *Int. J. Quantum Chem.*, 2019, **119**, e25705.
- 89 F. Pavošević, T. Culpitt and S. Hammes-Schiffer, Multicomponent Quantum Chemistry: Integrating Electronic and Nuclear Quantum Effects via the Nuclear–Electronic Orbital Method, *Chem. Rev.*, 2020, **120**, 4222–4253.
- 90 S. Hammes-Schiffer, Nuclear–electronic orbital methods: Foundations and prospects, *J. Chem. Phys.*, 2021, **155**, 030901.
- 91 M. V. Pak and S. Hammes-Schiffer, Electron-Proton Correlation for Hydrogen Tunneling Systems, *Phys. Rev. Lett.*, 2004, **92**, 103002.
- 92 M. V. Pak, C. Swalina, S. P. Webb and S. Hammes-Schiffer, Application of the nuclear–electronic orbital method to hydrogen transfer systems: multiple centers and multiconfigurational wavefunctions, *Chem. Phys.*, 2004, **304**, 227–236.
- 93 E. Kamarchik and D. A. Mazziotti, Coupled nuclear and electronic ground-state motion from variational reduced-density-matrix theory with applications to molecules with floppy or resonant hydrogens, *Phys. Rev. A*, 2009, **79**, 012502.
- 94 Q. Yu and S. Hammes-Schiffer, Nuclear-Electronic Orbital Multistate Density Functional Theory, *J. Phys. Chem. Lett.*, 2020, **11**, 10106–10113.
- 95 R. F. W. Bader, *Atoms in Molecules: A Quantum Theory*, Clarendon Press, 1994.
- 96 P. L. Popelier, *Atoms in Molecules: An Introduction*, Prentice Hall, Harlow, 1 edition., 2000.
- 97 C. F. Matta and R. J. Boyd, *The Quantum Theory of Atoms in Molecules: From Solid State to DNA and Drug Design*, Wiley-VCH, Weinheim, 2007.
- 98 P. Nasertayoob, M. Goli and S. Shahbazian, Toward a regional quantum description of the positronic systems: Primary considerations, *Int. J. Quantum Chem.*, 2011, **111**, 1970–1981.
- 99 M. Goli and S. Shahbazian, The quantum theory of atoms in positronic molecules: A case study on diatomic species, *Int. J. Quantum Chem.*, 2011, **111**, 1982–1998.
- 100 F. Heidar Zadeh and S. Shahbazian, The quantum theory of atoms in positronic molecules: The subsystem variational procedure, *Int. J. Quantum Chem.*, 2011, **111**, 1999–2013.
- 101 M. Goli and S. Shahbazian, Atoms in molecules: beyond Born–Oppenheimer paradigm, *Theor. Chem. Acc.*, 2011, **129**, 235–245.
- 102 M. Goli and S. Shahbazian, The two-component quantum theory of atoms in molecules (TC-QTAIM): foundations, *Theor. Chem. Acc.*, 2012, **131**, 1208.

- 103S. Shahbazian, Beyond the orthodox QTAIM: motivations, current status, prospects and challenges, *Found. Chem.*, 2013, **15**, 287–302.
- 104M. Goli and S. Shahbazian, The two-component quantum theory of atoms in molecules (TC-QTAIM): tensor formulation and its implications, *Theor. Chem. Acc.*, 2013, **132**, 1362.
- 105M. Goli and S. Shahbazian, Toward the multi-component quantum theory of atoms in molecules: a variational derivation, *Theor. Chem. Acc.*, 2013, **132**, 1365.
- 106M. Goli and S. Shahbazian, The two-component quantum theory of atoms in molecules (TC-QTAIM): the unified theory of localization/delocalization of electrons, nuclei, and exotic elementary particles, *Theor. Chem. Acc.*, 2013, **132**, 1410.
- 107M. Goli and S. Shahbazian, Deciphering the “chemical” nature of the exotic isotopes of hydrogen by the MC-QTAIM analysis: the positively charged muon and the muonic helium as new members of the periodic table, *Phys. Chem. Chem. Phys.*, 2014, **16**, 6602–6613.
- 108M. Goli and S. Shahbazian, Topological and AIM analyses beyond the Born–Oppenheimer paradigm: New opportunities, *Comput. Theor. Chem.*, 2015, **1053**, 96–105.
- 109M. Goli and S. Shahbazian, Hidden aspects of the Structural theory of chemistry: MC-QTAIM analysis reveals “alchemical” transformation from a triatomic to a diatomic structure, *Phys. Chem. Chem. Phys.*, 2015, **17**, 245–255.
- 110M. Goli and S. Shahbazian, Where to place the positive muon in the Periodic Table?, *Phys. Chem. Chem. Phys.*, 2015, **17**, 7023–7037.
- 111M. Goli and S. Shahbazian, Muon-Substituted Malonaldehyde: Transforming a Transition State into a Stable Structure by Isotope Substitution, *Chem. - Eur. J.*, 2016, **22**, 2525–2531.
- 112M. Goli and S. Shahbazian, Extending the Domain-Averaged Exchange-Correlation Energies Within the Context of the MC-QTAIM: Tracing Subtle Variations Induced by Isotope Substitution, *ChemPhysChem*, 2016, **17**, 3875–3880.
- 113M. Gharabaghi and S. Shahbazian, Incorporating nuclear vibrational energies into the “atom in molecules” analysis: An analytical study, *J. Chem. Phys.*, 2017, **146**, 154106.
- 114M. Goli and S. Shahbazian, Developing effective electronic-only coupled-cluster and Møller–Plesset perturbation theories for the muonic molecules, *Phys. Chem. Chem. Phys.*, 2018, **20**, 16749–16760.
- 115M. Goli and S. Shahbazian, On the Nature of the Positronic Bond, *ChemPhysChem*, 2019, **20**, 831–837.
- 116S. Shahbazian, in *Advances in Quantum Chemical Topology Beyond QTAIM*, eds. J. I. Rodríguez, F. Cortés-Guzmán and J. S. M. Anderson, Elsevier, 1st edn., 2022, pp. 73–109.
- 117S. Shahbazian, chapter in: *Comprehensive Computational Chemistry (Series of Reference Module in Chemistry, Molecular Sciences and Chemical Engineering)* Elsevier, 2022.
- 118P. L. A. Popelier and D. S. Kosov, Atom–atom partitioning of intramolecular and intermolecular Coulomb energy, *J. Chem. Phys.*, 2001, **114**, 6539–6547.
- 119M. A. Blanco, A. Martín Pendás and E. Francisco, Interacting Quantum Atoms: A Correlated Energy Decomposition Scheme Based on the Quantum Theory of Atoms in Molecules, *J. Chem. Theory Comput.*, 2005, **1**, 1096–1109.

- 120 E. Francisco, A. Martín Pendás and M. A. Blanco, A Molecular Energy Decomposition Scheme for Atoms in Molecules, *J. Chem. Theory Comput.*, 2006, **2**, 90–102.
- 121 J. M. Guevara-Vela, E. Francisco, T. Rocha-Rinza and Á. Martín Pendás, Interacting Quantum Atoms—A Review, *Molecules*, 2020, **25**, 4028.
- 122 A. F. Silva, L. J. Duarte and P. L. A. Popelier, Contributions of IQA electron correlation in understanding the chemical bond and non-covalent interactions, *Struct. Chem.*, 2020, **31**, 507–519.
- 123 M. V. Pak, A. Chakraborty and S. Hammes-Schiffer, Density Functional Theory Treatment of Electron Correlation in the Nuclear–Electronic Orbital Approach, *J. Phys. Chem. A*, 2007, **111**, 4522–4526.
- 124 A. Chakraborty, M. V. Pak and S. Hammes-Schiffer, Development of Electron-Proton Density Functionals for Multicomponent Density Functional Theory, *Phys. Rev. Lett.*, 2008, **101**, 153001.
- 125 A. Chakraborty, M. V. Pak and S. Hammes-Schiffer, Properties of the exact universal functional in multicomponent density functional theory, *J. Chem. Phys.*, 2009, **131**, 124115.
- 126 A. Sirjoosingh, M. V. Pak and S. Hammes-Schiffer, Derivation of an Electron–Proton Correlation Functional for Multicomponent Density Functional Theory within the Nuclear–Electronic Orbital Approach, *J. Chem. Theory Comput.*, 2011, **7**, 2689–2693.
- 127 A. Sirjoosingh, M. V. Pak and S. Hammes-Schiffer, Multicomponent density functional theory study of the interplay between electron-electron and electron-proton correlation, *J. Chem. Phys.*, 2012, **136**, 174114.
- 128 T. Culpitt, K. R. Brorsen, M. V. Pak and S. Hammes-Schiffer, Multicomponent density functional theory embedding formulation, *J. Chem. Phys.*, 2016, **145**, 044106.
- 129 K. R. Brorsen, Y. Yang and S. Hammes-Schiffer, Multicomponent Density Functional Theory: Impact of Nuclear Quantum Effects on Proton Affinities and Geometries, *J. Phys. Chem. Lett.*, 2017, **8**, 3488–3493.
- 130 Y. Yang, K. R. Brorsen, T. Culpitt, M. V. Pak and S. Hammes-Schiffer, Development of a practical multicomponent density functional for electron-proton correlation to produce accurate proton densities, *J. Chem. Phys.*, 2017, **147**, 114113.
- 131 K. R. Brorsen, P. E. Schneider and S. Hammes-Schiffer, Alternative forms and transferability of electron-proton correlation functionals in nuclear-electronic orbital density functional theory, *J. Chem. Phys.*, 2018, **149**, 044110.
- 132 Y. Yang, T. Culpitt and S. Hammes-Schiffer, Multicomponent Time-Dependent Density Functional Theory: Proton and Electron Excitation Energies, *J. Phys. Chem. Lett.*, 2018, **9**, 1765–1770.
- 133 Z. Tao, Y. Yang and S. Hammes-Schiffer, Multicomponent density functional theory: Including the density gradient in the electron-proton correlation functional for hydrogen and deuterium, *J. Chem. Phys.*, 2019, **151**, 124102.
- 134 U. Kuenzer, M. Klotz and T. S. Hofer, Probing vibrational coupling via a grid-based quantum approach—an efficient strategy for accurate calculations of localized normal modes in solid-state systems: Probing Vibrational Coupling via a Grid-Based Quantum Approach—An Efficient Strategy for Accurate Calculations of Localized Normal Modes in Solid-Stat, *J. Comput. Chem.*, 2018, **39**, 2196–2209.

- 135 U. Kuenzer and T. S. Hofer, A four-dimensional Numerov approach and its application to the vibrational eigenstates of linear triatomic molecules – The interplay between anharmonicity and inter-mode coupling, *Chem. Phys.*, 2019, **520**, 88–99.
- 136 M. J. Schuler, T. S. Hofer, Y. Morisawa, Y. Futami, C. W. Huck and Y. Ozaki, Solvation effects on wavenumbers and absorption intensities of the OH-stretch vibration in phenolic compounds – electrical- and mechanical anharmonicity via a combined DFT/Numerov approach, *Phys. Chem. Chem. Phys.*, 2020, **22**, 13017–13029.
- 137 M. Bollhöfer and Y. Notay, JADAMILU: a software code for computing selected eigenvalues of large sparse symmetric matrices, *Comput. Phys. Commun.*, 2007, **177**, 951–964.
- 138 T. H. Dunning, Gaussian basis sets for use in correlated molecular calculations. I. The atoms boron through neon and hydrogen, *J. Chem. Phys.*, 1989, **90**, 1007–1023.
- 139 A. D. Becke, Density-functional thermochemistry. III. The role of exact exchange, *J. Chem. Phys.*, 1993, **98**, 5648–5652.
- 140 Y. Yang, T. Culpitt, Z. Tao and S. Hammes-Schiffer, Stability conditions and local minima in multicomponent Hartree-Fock and density functional theory, *J. Chem. Phys.*, 2018, **149**, 084105.
- 141 F. Pavošević, T. Culpitt and S. Hammes-Schiffer, Multicomponent Coupled Cluster Singles and Doubles Theory within the Nuclear-Electronic Orbital Framework, *J. Chem. Theory Comput.*, 2019, **15**, 338–347.
- 142 M. W. Schmidt, K. K. Baldridge, J. A. Boatz, S. T. Elbert, M. S. Gordon, J. H. Jensen, S. Koseki, N. Matsunaga, K. A. Nguyen, S. Su, T. L. Windus, M. Dupuis and J. A. Montgomery, General atomic and molecular electronic structure system, *J. Comput. Chem.*, 1993, **14**, 1347–1363.
- 143 M. Goli and S. Shahbazian, Two-component density functional theory for muonic molecules: Inclusion of the electron–positive muon correlation functional, *J. Chem. Phys.*, 2022, **156**, 044104.
- 144 P. Maxwell, Á. M. Pendás and P. L. A. Popelier, Extension of the interacting quantum atoms (IQA) approach to B3LYP level density functional theory (DFT), *Phys. Chem. Chem. Phys.*, 2016, **18**, 20986–21000.
- 145 E. Francisco, J. L. Casals-Sainz, T. Rocha-Rinza and A. Martín Pendás, Partitioning the DFT exchange–correlation energy in line with the interacting quantum atoms approach, *Theor. Chem. Acc.*, 2016, **135**, 170.
- 146 P. Sanz, M. M. Montero-Campillo, O. Mó, M. Yáñez, I. Alkorta and J. Elguero, Intramolecular magnesium bonds in malonaldehyde-like systems: a critical view of the resonance-assisted phenomena, *Theor. Chem. Acc.*, 2018, **137**, 97.
- 147 S. Shahbazian, Why Bond Critical Points Are Not “Bond” Critical Points, *Chem. – Eur. J.*, 2018, **24**, 5401–5405.
- 148 C. Outeiral, M. A. Vincent, Á. M. Pendás and P. L. A. Popelier, Revitalizing the concept of bond order through delocalization measures in real space, *Chem. Sci.*, 2018, **9**, 5517–5529.
- 149 J. Charry, M. T. do N. Varella and A. Reyes, Binding Matter with Antimatter: The Covalent Positron Bond, *Angew. Chem. Int. Ed.*, 2018, **57**, 8859–8864.
- 150 T. Steiner, The Hydrogen Bond in the Solid State, *Angew. Chem. Int. Ed.*, 2002, **41**, 48–76.

Supporting Information

The MC-QTAIM analysis reveals an exotic bond in the coherently quantum superposed Malonaldehyde

Mohammad Goli¹ and Shant Shahbazian²

¹School of Nano Science, Institute for Research in Fundamental Sciences (IPM), Tehran

19395-5531, Iran,

Email: m_goli@ipm.ir

²Department of Physics, Shahid Beheshti University, Evin, Tehran, Iran

E-mail: sh_shahbazian@sbu.ac.ir

Table of contents

Page 34: The optimized geometry of **1** (or **3**) and **2** at the CCSD(T)/cc-pVQZ level

Page 35: The averaged geometries of **4** and **5**

Pages 36 and 37: The regression procedure: Transforming numerical proton wavefunctions into Gaussian-type orbitals

Page 38: Table S1- Summary of the ab initio NEO-DFT results

The optimized geometry of 1 (or 3) at the CCSD(T)/cc-pVQZ level				
Atom	Number	Coordinates [Bohr]		
		X	Y	Z
C	1	0.000000	2.077361	0.000000
C	2	2.339522	0.675322	0.000000
C	3	-2.236791	0.811101	0.000000
O	4	2.439903	-1.657362	0.000000
O	5	-2.441842	-1.681011	0.000000
H	6	0.019948	4.116154	0.000000
H	7	4.109976	1.763188	0.000000
H	8	-4.041823	1.778489	0.000000
H*	9	-0.688985	-2.333555	0.000000

* The coordinates of the quantum hydrogen atom

The optimized geometry of 2 at the CCSD(T)/cc-pVQZ level				
Atom	Number	Coordinates [Bohr]		
		X	Y	Z
C	1	0.000000	0.000000	2.130982
C	2	0.000000	-2.239563	0.731188
C	3	0.000000	2.239563	0.731188
O	4	0.000000	-2.229682	-1.682393
O	5	0.000000	2.229682	-1.682393
H	6	0.000000	0.000000	4.166644
H	7	0.000000	-4.079697	1.658786
H	8	0.000000	4.079697	1.658786
H*	9	0.000000	0.000000	-2.126078

* The coordinates of the quantum hydrogen atom

The averaged geometry of 4				
Atom	Number	Coordinates [Bohr]		
		X	Y	Z
C	1	0.000000	0.000000	4.458367
C	2	2.288822	0.000000	3.124956
C	3	-2.288822	0.000000	3.124956
O	4	2.439951	0.000000	0.711995
O	5	-2.439951	0.000000	0.711995
H	6	0.000000	0.000000	6.497257
H	7	4.077565	0.000000	4.152645
H	8	-4.077565	0.000000	4.152645
Bq*	9	-0.564373	0.000000	0.132820
Bq*	10	0.564373	0.000000	0.132820

* The coordinates of the “ghost atoms” used as the centers of expansion for the electronic basis functions of the quantum hydrogen atom coinciding with the maxima of the ground state protonic orbital.

The averaged geometry of 5				
Atom	Number	Coordinates [Bohr]		
		X	Y	Z
C	1	0.000000	0.000000	4.458367
C	2	2.288822	0.000000	3.124956
C	3	-2.288822	0.000000	3.124956
O	4	-2.439951	0.000000	0.711995
O	5	2.439951	0.000000	0.711995
H	6	0.000000	0.000000	6.497257
H	7	4.077565	0.000000	4.152645
H	8	-4.077565	0.000000	4.152645
Bq*	9	-0.582494	0.000000	0.121241
Bq*	10	0.582494	0.000000	0.121241

* The coordinates of the “ghost atoms” used as the centers of expansion for the electronic basis functions of the quantum hydrogen atom coinciding with the maxima of the excited state protonic orbital.

The regression procedure: Transforming the numerical protonic wavefunctions into the Gaussian-type orbitals

The numerical ground and excited protonic orbitals, obtained by the 3D Numerov method, were fitted by linear combinations of [6s6p6d] Cartesian Gaussian-type shells which were placed on the molecular symmetry plane of the averaged geometry that contains all the clamped nuclei. This is called the xz plane where the x-axis is the C_2 geometrical symmetry axis with respect to the rotation of the clamped nuclei. In the fitting procedure, the protonic orbital is explicitly shown by:

$$\Psi_{ground\ state} = \sum_{i=1}^{15} [c_i \varphi_{\alpha_i}(x_i, y_i, z_i) + c_i \varphi_{\alpha_i}(-x_i, y_i, z_i)],$$

and,

$$\Psi_{excited\ state} = \sum_{i=1}^{15} [c_i \varphi_{\alpha_i}(x_i, y_i, z_i) - c_i \varphi_{\alpha_i}(-x_i, y_i, z_i)],$$

where c_i , α_i and (x_i, y_i, z_i) are the coefficients, exponents and coordinates of the center of *i*-th normalized Gaussian function in these series, respectively. It must be noted that only non-zero contributions, due to the molecular symmetry, were included in the wavefunction expansions and offered in the forthcoming tables of the optimal parameters. The following tables gather the optimized parameters of the protonic orbitals, which were derived after the fitting of the Gaussian expansions to the 3D grid of the protonic wavefunctions.

Regression parameters of the ground state protonic orbital							
Function Number	Shell Number	Function Type	Exponent	Coefficient t	Coordinates [Bohr]		
					X	Y	Z
1	1	S	5.92536	-0.667308	0.098133	0.000000	-0.042515
2	2	S	4.90609	0.103662	0.831002	0.000000	-0.082282
3	3	S	5.53872	0.971034	0.256124	0.000000	-0.022740
4	4	Pz	9.99765	-0.025588	0.894294	0.000000	-0.102668
5	5	Pz	5.98643	0.277155	0.488342	0.000000	-0.086228
6	6	Pz	8.71275	-0.067002	0.668808	0.000000	0.221253
7	7	Dxx	6.17956	0.583140	0.559992	0.000000	0.043214
8	7	Dyy	6.17956	-0.405039	0.559992	0.000000	0.043214
9	7	Dzz	6.17956	0.505316	0.559992	0.000000	0.043214
10	8	Dxx	6.97638	0.417660	0.736994	0.000000	0.148422
11	8	Dyy	6.97638	-0.295682	0.736994	0.000000	0.148422
12	8	Dzz	6.97638	0.230332	0.736994	0.000000	0.148422
13	9	Dxx	6.33365	-0.999577	0.649366	0.000000	0.093094
14	9	Dyy	6.33365	0.756131	0.649366	0.000000	0.093094
15	9	Dzz	6.33365	-0.587118	0.649366	0.000000	0.093094

Regression parameters of the excited state protonic orbital							
Function Number	Shell Number	Function Type	Exponent	Coefficient t	Coordinates [Bohr]		
					X	Y	Z
1	1	S	7.94753	-0.995443	0.063433	0.000000	-0.199071
2	2	S	8.43716	0.469871	0.967696	0.000000	0.165908
3	3	S	6.71810	0.999654	0.280224	0.000000	-0.116529
4	4	Pz	6.37756	-0.778184	0.720576	0.000000	0.060806
5	5	Pz	7.81809	0.835965	0.545553	0.000000	0.019451
6	6	Pz	7.93854	0.155353	0.834297	0.000000	0.249593
7	7	Dxx	7.17292	0.272671	0.498309	0.000000	0.080944
8	7	Dyy	7.17292	0.310717	0.498309	0.000000	0.080944
9	7	Dzz	7.17292	0.434034	0.498309	0.000000	0.080944
10	8	Dxx	6.66305	-0.207159	0.560419	0.000000	0.028372
11	8	Dyy	6.66305	-0.999654	0.560419	0.000000	0.028372
12	8	Dzz	6.66305	-0.402189	0.560419	0.000000	0.028372
13	9	Dxx	6.30875	-0.468891	0.618625	0.000000	0.067678
14	9	Dyy	6.30875	0.861386	0.618625	0.000000	0.067678
15	9	Dzz	6.30875	0.019168	0.618625	0.000000	0.067678

Table S1- Summary of the ab initio NEO-DFT results.

Method/basis set System	B3LYP-EPC17-1/[cc-pVTZ:10s10p10d]	
	2	1 and 3
<i>Electronic kinetic energy</i>	265.577772	265.554369
<i>Proton's kinetic energy</i>	0.007718	0.007746
<i>Electron-electron potential energy</i>	261.422933	258.206955
<i>Proton-electron potential energy</i>	-13.233539	-12.654149
<i>electron-clamped nuclei potential energy</i>	-949.386639	-943.531760
<i>Proton-clamped nuclei potential energy</i>	12.255060	11.684860
<i>Clamped Nuclei-clamped Nuclei potential energy</i>	156.082444	153.453666
<i>Total energy</i>	-267.274253	-267.278314
<i>Virial ratio</i>	2.006359	2.006463
Method/basis set System	B3LYP/[cc-pVTZ:6s6p6d]	
	4	5
<i>Electronic kinetic energy</i>	265.443959	265.454513
<i>Proton's kinetic energy</i>	0.005092	0.005817
<i>Electron-electron potential energy</i>	258.213390	258.215910
<i>Proton-electron potential energy</i>	-12.401579	-12.396164
<i>electron-clamped nuclei potential energy</i>	-943.513438	-943.531044
<i>Proton-clamped nuclei potential energy</i>	11.709815	11.712679
<i>Clamped Nuclei-clamped Nuclei potential energy</i>	153.388670	153.388670
<i>Total energy</i>	-267.154092	-267.149620
<i>Virial ratio</i>	2.006423	2.006364